

Impact of Lipid Oxidization on Vertical Structures and Electrostatics of Phospholipid Monolayers Revealed by Combination of Specular X-ray Reflectivity and Grazing-Incidence X-ray Fluorescence

Agatha Korytowski,[†] Wasim Abuillan,[†] Ali Makky,^{†,‡} Oleg Konovalov,[§] and Motomu Tanaka^{*,†,||}

[†]Physical Chemistry of Biosystems, Physical Chemistry Institute, University of Heidelberg, 69120 Heidelberg, Germany

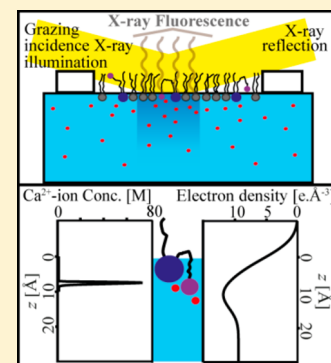
[‡]Institut Galien Paris Sud, Faculté de Pharmacie-Université Paris-Sud, 5 rue Jean-Baptiste Clément, 92296 Châtenay-Malabry, France

[§]European Synchrotron Radiation Facility (ESRF), Grenoble Cedex 9 38053, France

^{||}Institute for Integrated Cell-Material Sciences (iCeMS), Kyoto University, 606-8501 Kyoto, Japan

Supporting Information

ABSTRACT: The influence of phospholipid oxidization of floating monolayers on the structure perpendicular to the global plane and on the density profiles of ions near the lipid monolayer has been investigated by a combination of grazing incidence X-ray fluorescence (GIXF) and specular X-ray reflectivity (XRR). Systematic variation of the composition of the floating monolayers unravels changes in the thickness, roughness and electron density of the lipid monolayers as a function of molar fraction of oxidized phospholipids. Simultaneous GIXF measurements enable one to qualitatively determine the element-specific density profiles of monovalent (K^+ or Cs^+) and divalent ions (Ca^{2+}) in the vicinity of the interface in the presence and absence of two types of oxidized phospholipids (PazePC and PoxnoPC) with high spatial accuracy ($\pm 5 \text{ \AA}$). We found the condensation of Ca^{2+} near carboxylated PazePC was more pronounced compared to PoxnoPC with an aldehyde group. In contrast, the condensation of monovalent ions could hardly be detected even for pure oxidized phospholipid monolayers. Moreover, pure phospholipid monolayers exhibited almost no ion specific condensation near the interface. The quantitative studies with well-defined floating monolayers revealed how the elevation of lipid oxidation level alters the structures and functions of cell membranes.



1. INTRODUCTION

Mammalian phospholipids form lipid bilayers—the structural core of all biomembranes which are described in the mosaic model as a diffusion barrier and a structural matrix which embeds active molecules, peripheral and integral membrane proteins as well as covalently linked complex carbohydrates.¹ Phospholipids have mostly unsaturated acyl chains that are prone to oxidative damage at the location of the carbon–carbon double bonds. Phospholipids oxidization is initialized by lipid peroxidation which can be enzyme mediated or formed through reaction of lipids with reactive oxygen species including free radicals that are present in various tissues.² During the oxidation of lipids, carbonyl groups such as aldehydes, ketones, or carboxyl groups are formed through their structures and the oxidized alkyl chains become shorter and more polar.² As a consequence, such chemical modifications are very likely to change the physical properties of biological membranes such as the decrease in lipid order,³ the decrease in the PL melting temperature,⁴ the increase in the lipid mobility,⁵ and the alteration in the lateral phase organization.⁶ Thus, such products may alter the biological function of cell membrane as well its interaction with the surrounding environments including ions and proteins and may be the cause of several inflammatory^{7,8} and neurodegenerative diseases.^{9–11}

Among these oxidized phospholipids, PazePC and PoxnoPC are two stable lipid oxidation products originated from POPC oxidation. PazePC and PoxnoPC bear carboxyl and carbonyl groups respectively at the end of their truncated sn-2 chains. PoxnoPC is one of the key products of ozone mediated oxidation of lung surfactant extract¹² and promotes apoptosis and necrosis. PazePC has been detected in LDL particles and has been implicated in the genesis of atherosclerosis.¹³ At neutral pH, the carbonyl and carboxyl groups are zwitterionic and anionic, respectively. In addition, recent molecular dynamics simulation study¹⁴ suggests that a large free energy penalty of embedding a charged carboxyl group of PazePC in the hydrophobic core of a lipid bilayer induces the reversal of the oxidized chain into the aqueous phase. Although several studies have demonstrated the presence of oxidized phospholipids in many pathological states, there is no systematic study that unravels how lipid oxidation would influence the structures and electrostatics of cell membranes. Electrostatic information of membranes will lead to a better understanding of OxPL and their biological activity in apoptosis and necrosis in an ion specific environment.

Received: May 8, 2015

Revised: June 25, 2015

In the present work we investigate the impact of two oxidized phospholipids (PazePC and PoxnoPC) on the structures and electrostatics perpendicular to the global plane of phospholipids monolayers at the air/water interface using XRR and GIXF respectively in combination with compression isotherm measurements. XRR is widely used to reveal structures perpendicular to the surfaces for both hard and soft matters by measuring the momentum transfer normal to the sample plane. In addition to XRR, we performed GIXF by illuminating the samples across the critical angle of total reflection. GIXF has mostly been used to resolve the weak depletion of ions at the air/water interface¹⁵ and depth profile of Al impurities in Si wafers.¹⁶ Recently, GIXF has been used to reconstruct ion concentration profiles in the vicinity of lipopolysaccharide membrane surfaces.¹⁷ Therefore, the combination of XRR and GIXF would provide a comprehensive view of the electron density profiles perpendicular to the plane of floating monolayers, structure and form factor, and lateral concentration of ions penetrating into the monolayer surface.

II. MATERIALS AND METHODS

A. Materials and Sample Preparation. 1-(9Z-octadecenoyl)-2-hexadecanoyl-*sn*-glycero-3-phosphocholine (OPPC) was a generous gift from Lipoid (Ludwigshafen, Germany), and 1-palmitoyl-2-(9'-oxo-nonanoyl)-*sn*-glycero-3-phosphocholine (PoxnoPC) and 1-palmitoyl-2-azelaoyl-*sn*-glycero-3-phosphocholine (PazePC) were purchased from Avanti Polar Lipids (Alabaster, USA) (Figure 1). The stock solutions of lipid

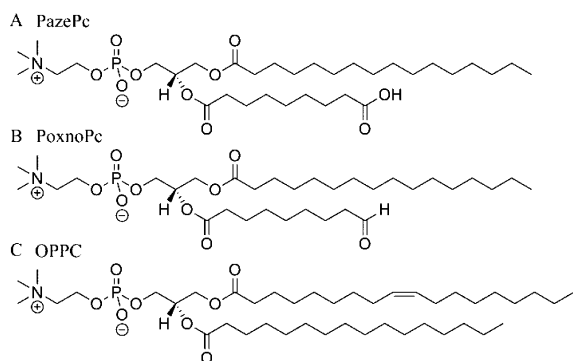


Figure 1. Chemical structures of PazePC (A), PoxnoPC (B), and OPPC (C).

mixtures at the final concentration of 1 mg/mL were prepared in chloroform and stored at $-20\text{ }^{\circ}\text{C}$. The purity of the above lipids was verified by thin layer chromatography on silica gel coated plates from Machery-Nagel (Düren, Germany), using chloroform/methanol/water/ammonia (65:20:2:2, v/v) as the eluent. No impurities were detected upon examination of the plates after potassium permanganate staining. Double deionized water (Milli-Q, Molsheim) with a specific resistance of $R > 18\text{ M}\Omega\text{cm}$ was used throughout this study. Monolayers were prepared by spreading the lipid solution onto the subphase. Prior to compression, 20 min was allowed for the complete evaporation of the solvent. The film was compressed to the surface pressure of $\pi = 20\text{ mN/m}$ which coincides with an area per lipid molecule in the range of $A \approx 65\text{--}110\text{ \AA}^2$, depending on the lipid mixture used.

In the present study, we studied the following systems; (i) pure OPPC (control), (ii) PazePC/OPPC (0.1), (iii) PoxnoPC/OPPC (0.1), (iv) pure PazePC, and (v) pure

PoxnoPC at the air/water interface. To investigate the influence of ion species on the structures and electrostatics of the interface, the monolayers were spread on (a) K^+ -buffer (150 mM KCl, 10 mM Hepes and 0.1 mM EDTA), (b) Ca^{2+} -buffer (75 mM CaCl_2 and 10 mM Hepes), and (c) Cs^+ -buffer (150 mM CsCl and 10 mM Hepes), and the pH was adjusted to 7.4 in all cases. XRR and GIXF measurements were carried out after each monolayer was compressed to the surface pressure of $\pi = 20\text{ mN/m}$.

B. XRR and GIXF Experiments. XRR and GIXF experiments were carried out at the beamline ID10B of the European Synchrotron Radiation Facility (ESRF, Grenoble, France). The samples were irradiated with a monochromatic synchrotron beam either with an energy of 8 keV ($\lambda = 1.55\text{ \AA}$), 9 keV ($\lambda = 1.37\text{ \AA}$), or 14 keV ($\lambda = 0.89\text{ \AA}$). The film balance was kept in a He atmosphere to minimize the scattering of the fluorescence emission by air as well as to minimize the radiation damage. Figure 2 represents a schematic drawing of the experimental setup and scattering geometry for XRR and GIXF experiments.

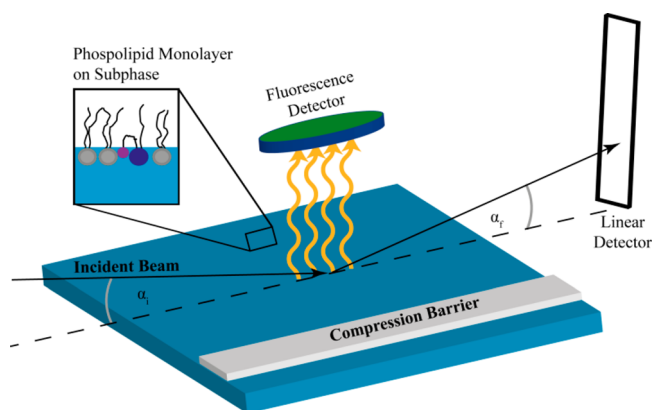


Figure 2. Experimental setup and the scattering geometry used for XRR and GIXF at the air/water interface.

XRR was measured with a linear detector (Vantec-1, Bruker AXS, USA). After subtraction of the diffuse intensity background (at $\alpha_f \neq \alpha_i$), the specular reflectivity was analyzed using the Parratt formalism¹⁸ with a genetic minimization algorithm implemented in the MOTOFIT software package.¹⁹

GIXF measurements were carried out at incident angles α_i below and above the critical angle of total reflection α_c . Here, the penetration depth of the evanescent field depends on the angle of incidence:²⁰

$$\Lambda(\alpha_i) = \frac{\lambda}{\sqrt{8\pi}} [\sqrt{(\alpha_i^2 - \alpha_c^2)^2 + 4\beta^2} - (\alpha_i^2 - \alpha_c^2)]^{-1/2} \quad (1)$$

where β is the imaginary part of the refractive index $n = 1 - \delta + i\beta$.

X-ray fluorescence signals from the chemical elements in the illuminated volume were recorded with an energy sensitive detector (Vortex, SII NanoTechnology, USA) and normalized by the detector counting efficiency. The emissions from K $K\alpha$, Ca $K\alpha$, or Cs $L\alpha$ lines were extracted using a multiple-Gaussian peak fitting routine in a self-written code (Igor Pro, WaveMetrics, Portland, USA). To compensate systematic differences between the experiments, the recorded fluorescence intensities were normalized by the elastically scattered beam

intensity. The fluorescence signals in the presence of monolayers were normalized by the signals from the corresponding blank buffer, and are plotted as a function of momentum transfer perpendicular to the interface, $q_z = 4\pi/\lambda \sin \alpha_i$. This procedure eliminates artifacts arising from the experimental geometry such as the size of beam footprint and the fluorescence detector aperture.¹⁷

C. Fluorescence Intensities for Stratified Interfaces.

Fluorescence intensity $I_i^f(\alpha)$ from a chemical element i at a distance z from the air/water interface at an incidence angle α can be written as

$$I_i^f(\alpha) = S \int_0^\infty I^{ill}(z, \alpha) c_i(z) \exp(-z/L_i) dz \quad (2)$$

S is a constant that is scaled out in our experimental system by the normalization to the fluorescence signal from the corresponding blank buffer, $c_i(z)$ is the concentration of element i at a depth z , and L_i is the attenuation length of water at the characteristic fluorescence line, e.g. $L_{K-\text{K}\alpha} = 68.14 \mu\text{m}$, $L_{\text{Ca}-\text{K}\alpha} = 93.71 \mu\text{m}$, and $L_{\text{Cs}-\text{L}\alpha} = 146.69 \mu\text{m}$. The illumination profile $I^{ill}(z, \alpha)$, which is the most crucial part for the quantitative GIXF analysis, can be determined by the matrix propagation technique²¹ using slabs model, yielding the electron density and the thicknesses of each slab.²²

The concentration profile of the ion species condensed at the phosphocholine headgroup of the lipid monolayer can be parametrized using an asymmetric Gaussian profile¹⁷

$$c_i(z) = c_0 + c_{\text{max}} \frac{\sqrt{e}(z - z_{\text{HC}})}{z_{\text{max}}} \exp\left(-\frac{(z - z_{\text{HC}})^2}{2z_{\text{max}}^2}\right) \quad (3)$$

where c_0 is the bulk concentration, z_{HC} the hydrocarbon chain/phosphocholine head interface, c_{max} the maximum ion concentration, and z_{max} its peak position. It should be noted that c_{max} and z_{max} are the only two fitting parameters in the fit. The analysis was refined with the Levenberg–Marquardt nonlinear least-squares optimization,²³ yielding the ion concentration profile along the z -axis. It should be noted that the XRR measurements are essential for the quantitative GIXF analysis, since the illumination profile I^{ill} (and thus the electromagnetic waves reflected/refracted in ultrathin films) strongly depends on their electronic structures.

III. RESULTS AND DISCUSSION

A. Impact of OxPI on OPPC Monolayers in the Presence of Monovalent K^+ Ions. Parts a–c of Figure 3 show the XRR curves of pure OPPC monolayer (black), OPPC monolayers doped with 10 mol % of PazePC/PoxnoPC (green), and pure PazePC/PoxnoPC monolayers (blue) on K^+ -buffer. The solid red line in each panel represents the best matching fits to the experimental data. The reconstructed electron density (ρ) profiles along the z -axis are also shown in Figure 3b–d. The thickness d , electron density ρ , and root-mean-square (rms) roughness σ of each interface are summarized in Table 1.

The hydrocarbon chain of pure OPPC has a thickness of $d_A = 11.7 \text{ \AA}$ with $\rho_A = 0.262 \text{ e \AA}^{-3}$. The ρ_A value is lower than those of saturated hydrocarbon chains $\rho_A = 0.32\text{--}0.33 \text{ e \AA}^{-3}$,^{24,25} while the total thickness of the monolayer (19.6 \AA) seems fully consistent with one-half of the values reported for the corresponding bilayers, 19.5 \AA .²⁶ Indeed, the average number of electrons per one phospholipid molecule calculated from the fit (440 e^-) is in good agreement with the one

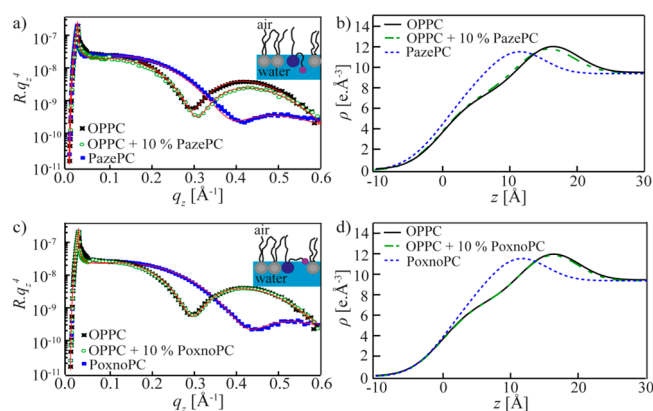


Figure 3. (a) XRR curves for OPPC (black), OPPC with 10 mol % PazePC (green) and pure PazePC (blue) on K^+ -buffer together with the best fits to the experimental results (solid red line) and a sketch of the $sm-2$ acyl chain reorientation of PazePC and PoxnoPC as an inlet, and (b) the reconstructed electron density profiles along the z -axis (perpendicular to the interface). The corresponding XRR and the electron density profiles from PoxnoPC systems are presented in parts c and d, respectively.

Table 1. Thickness d , Electron Density ρ , and Roughness σ Corresponding to Best Fits of the XRR of OPPC/OxPI Monolayers on K^+ Buffer at 20 mN/m

	d (Å)	ρ ($\text{e} \times \text{Å}^{-3}$)	σ (Å)
OPPC			
hydrocarbon chain	11.7	0.262	4.0
choline head	7.9	0.465	3.4
buffer	∞	0.335	3.3
OPPC + 10 mol % PazePC ^a			
hydrocarbon chain	11.4	0.263	4.1
choline head	7.4	0.460	3.6
buffer	∞	0.335	3.2
PazePC ^a			
hydrocarbon chain	7.7	0.322	4.5
choline head	6.6	0.454	3.5
buffer	∞	0.335	3.3
OPPC + 10 mol % PoxnoPC			
hydrocarbon chain	11.7	0.263	4.0
choline head	7.5	0.465	3.5
buffer	∞	0.335	3.3
PoxnoPC			
hydrocarbon chain	7.4	0.295	4.1
choline head	6.6	0.460	3.6
buffer	∞	0.335	3.2

^aThe membranes containing PazePC were less stable than those containing PoxnoPC.

calculated from the chemical formula of OPPC (420 e^-), which validates the quality of the fit.

It is notable that the hydrocarbon chains of both PazePC and PoxnoPC monolayers are about 4 \AA thinner compared to that of OPPC monolayer recorded at the same surface pressure. The smaller values found for the hydrocarbon chain layer thickness can be interpreted in terms of conformational change of the oxidized chains toward the aqueous phase,²⁷ followed by an increase in the mean molecular area. In fact, we observed the increase in molecular area with increasing molar fractions of OxPI (see Supporting Information, section S1). This results in the increase in the electron density of hydrocarbon chain ($\Delta\rho =$

10–20%) as well as the interface roughness. Such disturbance to the chain orders we observed seems consistent with the previous MD simulations of DOPC and POPC mixed with mono-oxidized acyl chain bearing an aldehyde group²⁸ as well as in MD simulations with PLPC mixed with an aldehyde group²⁹ where the tendency of the oxidized modified acyl chain to reorientate toward the water interface (Figure 3a–c, inlet) leads to an increase in the average area per lipid and a decrease in bilayer thickness with higher content of OxPI. In addition, the experimental finding from the fluorescence film balance (Sabbatini) shows film expansion of monolayers with increasing content of OxPI and a solubilization of the OxPI into the aqueous phase at high film compression.²⁷ However, when PazePC/PoxnoPC were incorporated into OPPC with 10 mol % (Figure 3a–c, green), the thickness, the roughness of each interface and the electron density of hydrocarbon chain layers showed no remarkable difference of the corresponding values from pure OPPC, suggesting that the incorporation of OxPI at 10 mol % leads to no remarkable change in the vertical structures of phospholipid monolayers.

B. Density Profiles of K^+ Ions in the Presence/Absence of OxPI. Figure 4 represents the normalized $K K_\alpha$ fluorescence

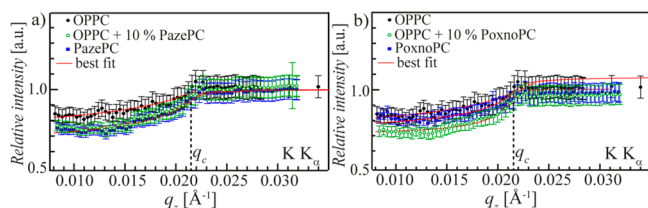


Figure 4. (a) Fluorescence intensities of $K K_\alpha$ as a function of q_z for OPPC (black), OPPC with 10 mol % PazePC (green) and pure PazePC (blue) on K^+ -buffer together with the best fits (solid red line). The corresponding fluorescence intensities from OPPC/PoxnoPC systems are presented in part b.

intensities for (a) OPPC/PazePC monolayers and (b) OPPC/PoxnoPC monolayers on K^+ -buffer. The red lines coincide with the best fit results. The fluorescence signals of $K K_\alpha$ are close to unity, indicating that K^+ ions are not enriched at the interface and K^+ ions are weakly interacting with all phospholipids that are subjected in this study. Although the slightly lower fluorescence signals at $q_z < q_c$ compared to unity seem to suggest a depletion of K^+ ions near the interface, the reconstructed ion concentration profiles in this case were equal to the bulk values by taking the modulation of electron densities at the air/water interface.

C. Impact of OxPI on OPPC Monolayer in the Presence of Divalent Ca^{2+} Ions. Figure 5 shows the XRR curves of OPPC/OxPI monolayers on Ca^{2+} -buffer together with the best fits to the reflectivity curves (red lines). The parameters corresponding to the best fit results are summarized in Table 2.

The OPPC monolayer on Ca^{2+} -buffer shows similar structural parameters to those on K^+ -buffer, suggesting that Ca^{2+} ions do not alter the structure of OPPC membranes. As presented in Figure 3, parts a and b, the incorporation of 10 mol % PazePC did not result in any remarkable change in thickness, electron density, and roughness of each interface. The same tendency was observed for the membrane incorporating 10 mol % of PoxnoPC, indicating that the structural integrity of OPPC membranes was not disturbed by the oxidation of hydrocarbon chains up to 10 mol %.

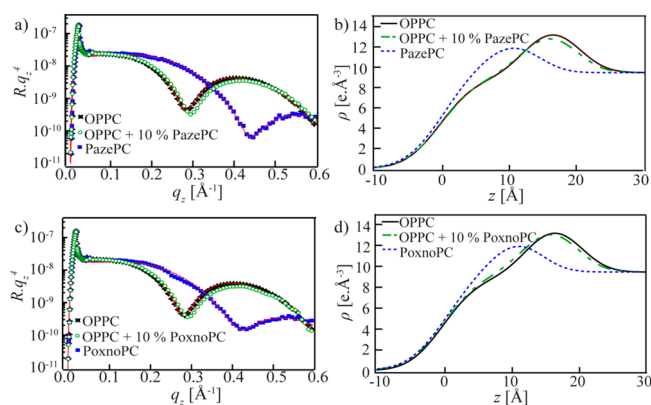


Figure 5. (a) XRR curves OPPC (black), OPPC with 10 mol % PazePC (green) and pure PazePC (blue) on Ca^{2+} -buffer together with the best fits to the experimental results (solid red line) and (b) the reconstructed electron density profiles along the z -axis (perpendicular to the interface). The corresponding XRR and the electron density profiles from OPPC/PoxnoPC systems are presented in parts c and d, respectively.

Table 2. Thickness d , Electron Density ρ , and Roughness σ Corresponding to Best Fits of the XRR of OPPC/OxPI Monolayers on Ca^{2+} -Buffer Measured at 20 mN/m

	d (Å)	ρ ($e \times \text{Å}^{-3}$)	σ (Å)
OPPC			
hydrocarbon chain	12.4	0.317	4.1
choline head	8.0	0.510	3.3
buffer	∞	0.335	3.2
OPPC + 10 mol % PazePC			
hydrocarbon chain	12.0	0.318	4.3
choline head	7.6	0.496	3.4
buffer	∞	0.335	3.2
PazePC			
hydrocarbon chain	7.6	0.352	4.3
choline head	6.3	0.478	4.2
buffer	∞	0.335	3.2
OPPC + 10 mol % PoxnoPC			
hydrocarbon chain	12.0	0.319	4.3
choline head	7.8	0.502	3.5
buffer	∞	0.335	3.2
PoxnoPC			
hydrocarbon chain	7.9	0.333	4.3
choline head	6.2	0.473	3.6
buffer	∞	0.335	3.2

We also found that the monolayers of pure PazePC and pure PoxnoPC (blue) were thinner than OPPC monolayers; $\Delta d_A \sim -4.6$ Å for hydrocarbon chains and $\Delta d_H = -1.8$ Å for head groups. This finding follows the same tendency we found on K^+ -buffer for the monolayer thickness. But on the other hand, the PazePC and PoxnoPC monolayers on Ca^{2+} -buffer possess much larger electron densities for headgroup and hydrocarbon chain regions compared to that on K^+ -buffer. This suggests one of the following two scenarios: either lipid molecules are laterally compacted on Ca^{2+} -buffer, or Ca^{2+} ions are enriched at the interface. The former scenario is less dominant, since the difference in area per lipid molecule at $\pi = 20$ mN/m between K^+ -buffer and Ca^{2+} -buffer is below 7% and the lateral compressibility is almost identical in the presence and absence of Ca^{2+} ions (see Supporting Information, sections S1, S2, and S3). In contrast, a remarkable increase in the electron density in

the slab of PazePC head groups was identified from XRR, which gives supporting evidence to the second scenario. The average number of electrons per one PazePC molecule calculated from the fit on Ca^{2+} -buffer ($N_e = 625 e^-$) was much larger than the value calculated from the chemical formula ($N_e = 364 e^-$), suggesting the cross-linking of lipids by Ca^{2+} ions (See Supporting Information S10). The enhanced lateral cooperativity in lipid monolayers in the presence of Ca^{2+} seems to be qualitatively in good agreement with the previous studies using ^2H NMR,³⁰ grazing incidence X-ray diffraction and Monte Carlo simulations,³¹ dilational rheology,³² and atomistic MD simulations.^{33,34,30}

D. GIXF-Impact of Divalent Ca^{2+} Ions on the Electrostatics of OPPC/OxPI Monolayers. To verify the condensation of Ca^{2+} ions at interfaces, we measured the density profiles of Ca^{2+} ions using GIXF. Figure 6a represents the

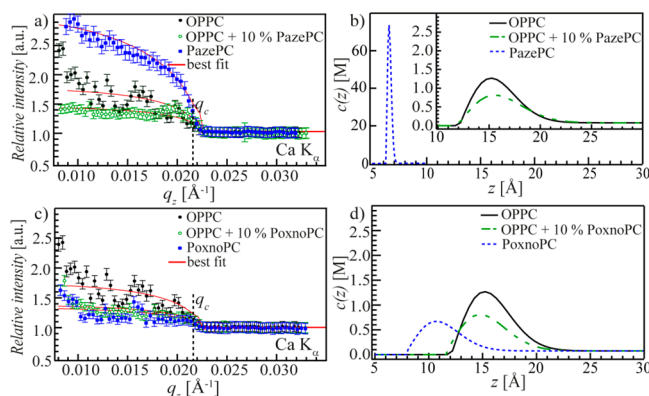


Figure 6. (a) Fluorescence intensities of $\text{Ca} K_{\alpha}$ as a function of q_z for OPPC (black), OPPC with 10 mol % PazePC (green) and pure PazePC (blue) on Ca^{2+} -buffer together with the best fits (solid red line) and the reconstructed ion concentration profiles (b). The corresponding results for OPPC/PoxnoPC systems are presented in parts c and d, respectively.

normalized $\text{Ca} K_{\alpha}$ fluorescence intensities for OPPC (black), OPPC with 10 mol % PazePC (green) and pure PazePC (blue) on Ca^{2+} -buffer. The red lines coincide with the best fit results. The reconstructed ion concentration profiles normal to the monolayer surfaces are presented in Figure 6b. The corresponding results for OPPC/PoxnoPC monolayers are presented in Figure 6, parts c and d, respectively. The parameters obtained from the best fit are summarized in Table 3.

The fluorescence signals at $q_z < q_c$ for all OPPC/PoxnoPC and OPPC/PazePC monolayers is higher than the bulk level (at $q_z > q_c$). This indicates that Ca^{2+} ions accumulate on the surface

Table 3. Positions of the Maximum Concentration z , Ion Lateral Concentration c_L , and Number of Ions per Lipid N of OPPC/OxPI Monolayers on Ca^{2+} -Buffer

	z (Å)	c_L (ions/cm ²) (10 ¹³)	N (ions/lipid)
OPPC	15.3	4.1	0.26
OPPC + 10 mol % PazePC	15.3	2.9	0.24
PazePC	6.6	19.0	2.1
OPPC + 10 mol % PoxnoPC	14.8	2.8	0.20
PoxnoPC	10.7	2.1	0.20

of phospholipid monolayers, which is consistent with the modification in electron densities suggested by XRR results.

In the absence of OxPI (black), the positions of the maximum concentration is located at $z_{\text{max}} = 15.3 \text{ Å}$ for OPPC, suggesting that Ca^{2+} ions are concentrated at the headgroup region. It should be noted that $z = 0$ is defined at the interface between air and hydrocarbon chains and thus the peak position is $15.3 - 12.8 = 2.5 \text{ Å}$ from the water surface. The obtained surface concentration (4.1×10^{13} ions/cm²) implies that $N = 0.26 \times \text{Ca}^{2+}$ ion is coupled to one OPPC molecule, i.e., $1 \times \text{Ca}^{2+}$ ion is coupled to $\sim 4 \times$ OPPC molecules. The incorporation of 10 mol % of PazePC/PoxnoPC (green) does not cause any remarkable change in the density profiles of Ca^{2+} near the interface; $z_{\text{max}} = 14.8 - 15.3 \text{ Å}$ and $N = 0.20 - 0.25$. In contrast, a remarkable enhancement of $\text{Ca} K_{\alpha}$ signals below q_c in a pure PazePC monolayer indicates a significant condensation of Ca^{2+} ions in the vicinity of interface, where the lateral Ca^{2+} ion concentration $c_L = 19 \times 10^{13}$ ions/cm² yields the 10 times larger number of Ca^{2+} ions per lipid molecule, $N = 2.1$. The finding that Ca^{2+} can bind to around four lipid headgroups or form lipid/ion clusters,³⁵ indicates that the enrichment of Ca^{2+} ions at the headgroup region can be explained by the high attractive interaction of the Ca^{2+} ions with the negatively charged carboxyl group of PazePC, which shows an acyl chain reversal into the aqueous phase as reported from MD simulations by Khandelia et al.¹⁴ On the other hand, a pure PoxnoPC monolayer (Figure 4, parts c and d, blue) showed a low Ca^{2+} ion condensation near the interface, where the number of Ca^{2+} ions coupled to one lipid $N = 0.20$ is comparable to those from the other conditions.

E. Impact of OxPI on OPPC Monolayers in the Presence of Monovalent Cs^+ Ions. The influence of size monovalent cations was further investigated by depositing monolayers on Cs^+ -buffer. Figure 7a,b represents the XRR

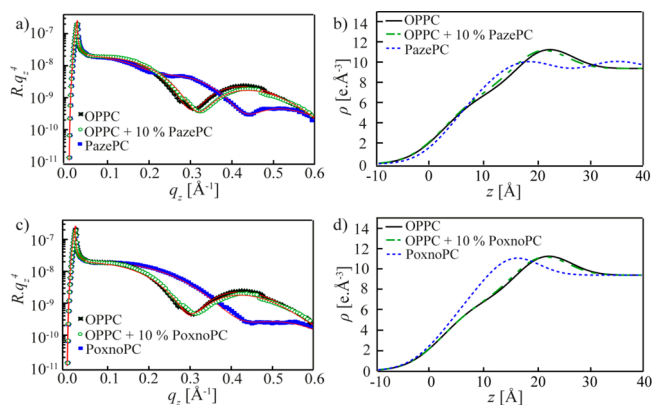


Figure 7. (a) XRR curves OPPC (black), OPPC with 10 mol % PazePC (green) and pure PazePC (blue) on Cs^+ -buffer together with the best fits to the experimental results (solid red line) and (b) the reconstructed electron density profiles along the z -axis (perpendicular to the interface). The corresponding XRR and the electron density profiles from PoxnoPC systems are presented in parts c and d, respectively.

curves of OPPC/OxPI monolayers together with the best fits to the reflectivity curves (red lines) for OPPC (black), OPPC with 10 mol % PazePC/PoxnoPC (green) and pure PazePC/PoxnoPC (blue) on Cs^+ -buffer. The reconstructed electron density profiles along the z -axis are presented in Figure 7c,d. The obtained thickness d , electron density ρ , and root-mean-

square (rms) roughness σ of each interface are summarized in Table 4.

Table 4. Thickness d , Electron Density ρ , and Roughness σ Corresponding to Best Fits of the XRR of OPPC/OxPI Monolayers on Cs⁺-Buffer Measured at 20 mN/m

	d (Å)	ρ ($e \times \text{Å}^{-3}$)	σ (Å)
OPPC			
hydrocarbon chain	11.3	0.253	4.4
choline head	7.3	0.437	3.4
buffer	∞	0.335	3.2
OPPC + 10 mol % PazePC			
hydrocarbon chain	10.7	0.260	4.4
choline head	7.1	0.436	3.4
buffer	∞	0.335	3.2
PazePC ^a			
hydrocarbon chain	6.6	0.302	3.9
choline head	5.8	0.384	4.1
buffer	∞	0.335	3.3
OPPC + 10 mol % PoxnoPC			
hydrocarbon chain	10.9	0.253	4.4
choline head	7.2	0.437	3.4
buffer	∞	0.335	3.2
PoxnoPC			
hydrocarbon chain	7.0	0.287	4.4
choline head	6.5	0.451	3.3
buffer	∞	0.335	3.2

^aValues for the PazePC monolayer from a 4-slab model.

The thickness and electron density values obtained for OPPC monolayers on Cs⁺-buffer in the presence and absence of OxPI are slightly but distinctly smaller than the corresponding values collected on K⁺-buffer. However, pure PoxnoPC monolayers on Cs⁺-buffer exhibited no distinguishable difference from that on K⁺-buffer. This finding suggests that the packing of negatively charged PazePC molecules becomes weaker by replacing K⁺-ions by the bulkier Cs⁺ ions, but uncharged PoxnoPC molecules are not influenced. It is notable that we could not detect any distinguishable difference in the lateral compressibility modulus (see Supporting Information, section S1). This seems to be in qualitative agreement with MD simulations of Jurkiewicz et al. on lipid bilayers, suggesting that the thickness of a bilayer in 1 M CsCl is distinctly thinner than those in 1 M KCl and NaCl, especially for membranes incorporating negatively charged phosphatidylserine (PS). Therefore, the difference in the structures of floating monolayers perpendicular to the global plane in the presence of Cs⁺ and K⁺ detected by XRR suggests that electrostatics of charged PazePC monolayers is influenced not only by valence numbers but also species of ions.

It should be noted that due to the weaker lateral packing, the pure PazePC monolayer was much more unstable than the other systems. The best matching fit to the XRR results could be achieved only by using a 4 slab model assuming the formation of aggregates of PazePC underneath the PazePC monolayer, as reported previously by Sabatini et al.³⁶

F. GIXF-Impact of Monovalent Cs⁺ Ions on the Electrostatics of OPPC/OxPI Monolayers. Figure 8a shows the normalized Cs $L\alpha$ fluorescence intensities OPPC (black), OPPC with 10 mol % PazePC (green) and pure PazePC (blue) on Cs⁺-buffer together with the best fit results

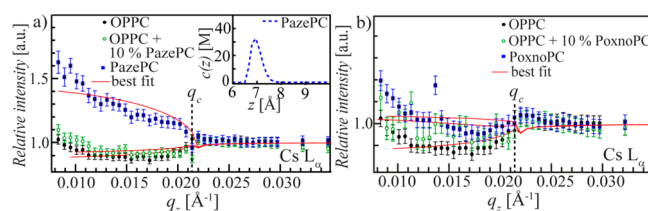


Figure 8. (a) Fluorescence intensities of Cs $L\alpha$ as a function of q_z for OPPC (black), OPPC with 10 mol % PazePC (green) and pure PazePC (blue) on Cs⁺-buffer together with the best fits (solid red line). The corresponding results for OPPC/PoxnoPC systems are presented in part b.

(red lines). The corresponding results for OPPC/PoxnoPC monolayers are presented in Figure 8b.

Like the case of monolayers on K⁺-buffer, the fluorescence intensities from OPPC (Figure 8, black) and OPPC doped with 10 mol % PazePC (Figure 8a, green) exhibit no sign of ion condensation near the interface. On the other hand, the signal from pure PazePC monolayer (Figure 8a, blue) is 1.5 times larger than the bulk signal. The reconstructed concentration profile presented as an inset in Figure 8a suggests the concentration maximum is located at $z = 7.0$ Å. Integrating the area under the curve yields the lateral concentration of Cs⁺ ions to be $c_L = 1.09 \times 10^{14}$ ions/cm². Considering the area per molecule corresponding to the experimental condition $A = 105$ Å² (SI), one can calculate the number of Cs⁺ ions per one PazePC molecule to be $N = 1.2$, suggesting that the binding stoichiometry of Cs⁺ and PazePC is almost 1:1, i.e. Cs⁺ does not cross-link PazePC molecules. This value is one-half of PazePC on Ca²⁺-buffer ($N = 2.1$). Namely, if one considers the valency, the binding affinity of PazePC to Cs⁺ is 4 times weaker than the binding to Ca²⁺. Remarkably, the number of Cs⁺ ions per PazePC molecule is about 5–6 times larger than the corresponding value for OPPC on Ca²⁺-buffer ($N = 0.20$ – 0.25). In contrast, the fluorescence signals from PoxnoPC-containing monolayers are close to unity (Figure 8b), indicating that ions are not concentrated near the interface. Although the sequence of binding affinity suggested by our GIXF results (Ca²⁺ > Cs⁺ > K⁺) is slightly different from what one expects from the Hofmeister series (Ca²⁺ > K⁺ > Cs⁺),^{37,35} this finding seems qualitatively consistent with XRR results where PazePC monolayer on Cs⁺-buffer was thinner than that on K⁺-buffer.

IV. SUMMARY AND CONCLUSION

In this work, we investigated the influence of oxidized phospholipids (PoxnoPC and PazePC) on the structures perpendicular to the global plane and density profiles ions (K⁺, Ca²⁺, Cs⁺) by the combination of XRR and GIXF at the air/water interface. Our XRR results on different buffers clearly indicated that both oxidized phospholipids form thinner monolayers than that of pure OPPC monolayer. Moreover, the doping of OxPIs (10 mol %) into OPPC already resulted in the thinning of floating monolayers, which was more pronounced for PazePC. Concerning the interaction with ions (monovalent and divalent ions), we observed strong specific effects of cations on mixed OPPC/OxPI monolayers. The reconstruction of ion-specific density profiles enables one to identify differences between different ions. For example, the thickness and stability of PazePC monolayers on Cs⁺-buffer were distinctly less than those on K⁺-buffer. Moreover, we found a clear enrichment of Cs⁺ in the vicinity of PazePC

membranes, while K^+ showed no sign of enrichment. The presence of Ca^{2+} cations thus has a significant effect shown (1) in an accumulation of Ca^{2+} ions near the head groups and (2) in increased thicknesses and increased electron densities of both hydrocarbon chains and choline heads of the monolayers. It is shown here that the *sn*-2 chain of PazePC with its carboxylic group is reversed into the subphase shows an accumulation of Ca^{2+} ions in polar head regions. From the experimental results, we calculated the number of $N = 2.1 \pm 0.1$ Ca^{2+} ions per PazePC lipid. However, PoxnoPC with its polar aldehyde group at the *sn*-2 chain, which is assumed to be reorientated toward the interface, did show an enhanced accumulation of Ca^{2+} ions in the head polar groups vicinity which is as large as for the pure matrix lipid (OPPC) monolayer, exhibiting much poorer ion specificity. The combination of XRR and GXF enables one to simultaneously gain both structures and ion specific density profiles perpendicular to the global plane of floating monolayers in high spatial accuracy (± 5 Å), which cannot be achieved by other optical techniques.

■ ASSOCIATED CONTENT

● Supporting Information

Pressure–area isotherms, compressional modulus and Gibbs free energy (section S1); influence of Ca^{2+} ions on the pressure–area isotherms (section S2); experimental values of the area per molecule at 20 mN/m (section S3); calculation of the number of electrons (section S4). The Supporting Information is available free of charge on the ACS Publications website at DOI: 10.1021/acs.jpcc.5b04451.

■ AUTHOR INFORMATION

Corresponding Author

*Telephone: +49-(0)-6221-544917. Fax: +49-(0)-6221-54 4918. E-mail tanaka@uni-heidelberg.de (M.T.).

Notes

The authors declare no competing financial interest.

■ ACKNOWLEDGMENTS

We thank ESRF for synchrotron beam time, and A. Körner, S. Inoue, A. Burk, N. Frenkel and A. Yamamoto for experimental help. A. K., A. M., and M. T. are thankful to P. K. J. Kinnunen for insightful comments. This work was supported by the Phospholipid Research Center (No. 120300), KAKENHI (No. 26103521 and 26247070). A. M. thanks Alexander von Humboldt Foundation for the postdoctoral fellowship. M. T. is a member of the German Excellence Cluster “CellNetwork”. The iCeMS is supported by World Premier International Research Center Initiative (WPI), MEXT, Japan.

■ ABBREVIATIONS

GXF, grazing-incidence X-ray fluorescence; XRR, specular X-ray reflectivity; OxPl, oxidized phospholipids; OPPC, 1-(9Z-octadecenoyl)-2-hexadecanoyl-*sn*-glycero-3-phosphocholine; PoxnoPC, 1-palmitoyl-2-(9'-oxo-nonanoyl)-*sn*-glycero-3-phosphocholine; PazePC, 1-palmitoyl-2-azelaoyl-*sn*-glycero-3-phosphocholine

■ REFERENCES

(1) Singer, S. J.; Nicolson, G. L. The Fluid Mosaic Model of the Structure of Cell Membranes. *Science* **1972**, *175*, 720–731.

(2) Hazen, S. L. Oxidized Phospholipids as Endogenous Pattern Recognition Ligands in Innate Immunity. *J. Biol. Chem.* **2008**, *283*, 15527–15531.

(3) Wratten, M. L.; Van Ginkel, G.; Van't Veld, A. A.; Bekker, A.; Van Faassen, E. E.; Sevanian, A. Structural and Dynamic Effects of Oxidatively Modified Phospholipids in Unsaturated Lipid Membranes. *Biochemistry* **1992**, *31*, 10901–10907.

(4) Megli, F. M.; Russo, L.; Conte, E. Spin Labeling Epr Studies of the Properties of Oxidized Phospholipid-Containing Lipid Vesicles. *Biochim. Biophys. Acta, Biomembr.* **2009**, *1788*, 371–379.

(5) Volinsky, R.; Cwiklik, L.; Jurkiewicz, P.; Hof, M.; Jungwirth, P.; Kinnunen, P. K. Oxidized Phosphatidylcholines Facilitate Phospholipid Flip-Flop in Liposomes. *Biophys. J.* **2011**, *101*, 1376–1384.

(6) Kinnunen, P. K. Fusion of Lipid Bilayers: A Model Involving Mechanistic Connection to H_{ii} Phase Forming Lipids. *Chem. Phys. Lipids* **1992**, *63*, 251–258.

(7) Berliner, J. A.; Heinecke, J. W. The Role of Oxidized Lipoproteins in Atherogenesis. *Free Radical Biol. Med.* **1996**, *20*, 707–727.

(8) Wood, L. G.; Gibson, P.; Garg, M. Biomarkers of Lipid Peroxidation, Airway Inflammation and Asthma. *Eur. Respir. J.* **2003**, *21*, 177–186.

(9) Dexter, D.; Carter, C.; Wells, F.; Javoy-Agid, F.; Agid, Y.; Lees, A.; Jenner, P.; Marsden, C. D. Basal Lipid Peroxidation in Substantia Nigra Is Increased in Parkinson's Disease. *J. Neurochem.* **1989**, *52*, 381–389.

(10) Markesbery, W. R. Oxidative Stress Hypothesis in Alzheimer's Disease. *Free Radical Biol. Med.* **1997**, *23*, 134–147.

(11) Zhang, X. Y.; Tan, Y. L.; Cao, L. Y.; Wu, G. Y.; Xu, Q.; Shen, Y.; Zhou, D. F. Antioxidant Enzymes and Lipid Peroxidation in Different Forms of Schizophrenia Treated with Typical and Atypical Antipsychotics. *Schizophr. Res.* **2006**, *81*, 291–300.

(12) Uhlson, C.; Harrison, K.; Allen, C. B.; Ahmad, S.; White, C. W.; Murphy, R. C. Oxidized Phospholipids Derived from Ozone-Treated Lung Surfactant Extract Reduce Macrophage and Epithelial Cell Viability. *Chem. Res. Toxicol.* **2002**, *15*, 896–906.

(13) Tokumura, A.; Toujima, M.; Yoshioka, Y.; Fukuzawa, K. Lipid Peroxidation in Low Density Lipoproteins from Human Plasma and Egg Yolk Promotes Accumulation of 1-Acyl Analogs of Platelet-Activating Factor-Like Lipids. *Lipids* **1996**, *31*, 1251–1258.

(14) Khandelia, H.; Mouritsen, O. G. Lipid Gymnastics: Evidence of Complete Acyl Chain Reversal in Oxidized Phospholipids from Molecular Simulations. *Biophys. J.* **2009**, *96*, 2734–2743.

(15) Padmanabhan, V.; Daillant, J.; Belloni, L.; Mora, S.; Alba, M.; Konovalov, O. Specific Ion Adsorption and Short-Range Interactions at the Air Aqueous Solution Interface. *Phys. Rev. Lett.* **2007**, *99*, 086105.

(16) Kayser, Y.; Banaś, D.; Cao, W.; Dousse, J.-C.; Hoszowska, J.; Jagodziński, P.; Kavčič, M.; Kubala-Kukuś, A.; Nowak, S.; Pajek, M. Depth Profiles of Al Impurities Implanted in Si Wafers Determined by Means of the High-Resolution Grazing Emission X-Ray Fluorescence Technique. *Spectrochim. Acta, Part B* **2010**, *65*, 445–449.

(17) Schneck, E.; Schubert, T.; Konovalov, O. V.; Quinn, B. E.; Gutsmann, T.; Brandenburg, K.; Oliveira, R. G.; Pink, D. A.; Tanaka, M. Quantitative Determination of Ion Distributions in Bacterial Lipopolysaccharide Membranes by Grazing-Incidence X-Ray Fluorescence. *Proc. Natl. Acad. Sci. U. S. A.* **2010**, *107*, 9147–9151.

(18) Parratt, L. G. Surface Studies of Solids by Total Reflection of X-Rays. *Phys. Rev.* **1954**, *95*, 359.

(19) Nelson, A. Co-Refinement of Multiple-Contrast Neutron/X-Ray Reflectivity Data Using Motofit. *J. Appl. Crystallogr.* **2006**, *39*, 273–276.

(20) Yun, W. B.; Bloch, J. M. X-Ray near Total External Fluorescence Method - Experiment and Analysis. *J. Appl. Phys.* **1990**, *68*, 1421–1428.

(21) Ohta, K.; Ishida, H. Matrix Formalism for Calculation of Electric Field Intensity of Light in Stratified Multilayered Films. *Appl. Opt.* **1990**, *29*, 1952–1959.

(22) Abuillan, W.; Schneck, E.; Korner, A.; Brandenburg, K.; Gutsmann, T.; Gill, T.; Vorobiev, A.; Konovalov, O.; Tanaka, M.

Physical Interactions of Fish Protamine and Antisepsis Peptide Drugs with Bacterial Membranes Revealed by Combination of Specular X-Ray Reflectivity and Grazing-Incidence X-Ray Fluorescence. *Phys. Rev. E* **2013**, *88*, 012705.

(23) Boggs, P. T.; Donaldson, J. R.; Schnabel, R. B. Algorithm 676: Odrpack: Software for Weighted Orthogonal Distance Regression. *ACM Trans. Math. Software* **1989**, *15*, 348–364.

(24) Majewski, J.; Kuhl, T.; Kjaer, K.; Smith, G. Packing of Ganglioside-Phospholipid Monolayers: An X-Ray Diffraction and Reflectivity Study. *Biophys. J.* **2001**, *81*, 2707–2715.

(25) Weygand, M.; Wetzer, B.; Pum, D.; Sleytr, U. B.; Cuvillier, N.; Kjaer, K.; Howes, P. B.; Lösche, M. Bacterial S-Layer Protein Coupling to Lipids: X-Ray Reflectivity and Grazing Incidence Diffraction Studies. *Biophys. J.* **1999**, *76*, 458–468.

(26) Vogel, M.; Münster, C.; Fenzl, W.; Salditt, T. Thermal Unbinding of Highly Oriented Phospholipid Membranes. *Phys. Rev. Lett.* **2000**, *84*, 390.

(27) Sabatini, K.; Mattila, J.-P.; Megli, F. M.; Kinnunen, P. K. Characterization of Two Oxidatively Modified Phospholipids in Mixed Monolayers with DPPC. *Biophys. J.* **2006**, *90*, 4488–4499.

(28) Cwiklik, L.; Jungwirth, P. Massive Oxidation of Phospholipid Membranes Leads to Pore Creation and Bilayer Disintegration. *Chem. Phys. Lett.* **2010**, *486*, 99–103.

(29) Wong-Ekkabut, J.; Xu, Z.; Triampo, W.; Tang, L.; Peter Tieleman, D.; Monticelli, L. Effect of Lipid Peroxidation on the Properties of Lipid Bilayers: A Molecular Dynamics Study. *Biophys. J.* **2007**, *93*, 4225–4236.

(30) Huster, D.; Jin, A. J.; Arnold, K.; Gawrisch, K. Water Permeability of Polyunsaturated Lipid Membranes Measured by ^{17}O NMR. *Biophys. J.* **1997**, *73*, 855–864.

(31) Oliveira, R. G.; Schneck, E.; Quinn, B. E.; Konovalov, O. V.; Brandenburg, K.; Gutschmann, T.; Gill, T.; Hanna, C. B.; Pink, D. A.; Tanaka, M. Crucial Roles of Charged Saccharide Moieties in Survival of Gram Negative Bacteria against Protamine Revealed by Combination of Grazing Incidence X-Ray Structural Characterizations and Monte Carlo Simulations. *Phys. Rev. E* **2010**, *81*, 041901.

(32) Makino, M.; Yoshikawa, K. Dynamic Properties of a Phospholipid Thin Film at an Air/Water Interface with a Periodic Change in Surface Area. *Langmuir* **1997**, *13*, 7125–7134.

(33) Böckmann, R. A.; Grubmüller, H. Multistep Binding of Divalent Cations to Phospholipid Bilayers: A Molecular Dynamics Study. *Angew. Chem., Int. Ed.* **2004**, *43*, 1021–1024.

(34) Huster, D.; Arnold, K.; Gawrisch, K. Strength of Ca^{2+} Binding to Retinal Lipid Membranes: Consequences for Lipid Organization. *Biophys. J.* **2000**, *78*, 3011–3018.

(35) Jurkiewicz, P.; Cwiklik, L.; Vojtišková, A.; Jungwirth, P.; Hof, M. Structure, Dynamics, and Hydration of POPC/Pops Bilayers Suspended in NaCl, KCl, and CsCl Solutions. *Biochim. Biophys. Acta, Biomembr.* **2012**, *1818*, 609–616.

(36) Sabatini, K.; Mattila, J.-P.; Megli, F. M.; Kinnunen, P. K. J. Characterization of Two Oxidatively Modified Phospholipids in Mixed Monolayers with DPPC. *Biophys. J.* **2006**, *90*, 4488–4499.

(37) Hofmeister, F. *Zur Lehre Von Der Wirkung Der Salze*; Springer: Berlin, 1888.